



Disrupted hypothalamic CRH neuron responsiveness contributes to diet-induced obesity

Canjun Zhu^{1,2}, Yuanzhong Xu², Zhiying Jiang², Jin Bin Tian^{2,3}, Ryan M Cassidy^{2,4}, Zhao-Lin Cai^{5,6}, Gang Shu¹ , Yong Xu⁷, Mingshan Xue^{5,6}, Benjamin R Arenkiel⁸, Qingyan Jiang^{1,*} & Qingchun Tong^{2,4,9,**} 

Abstract

The current obesity epidemic mainly results from high-fat high-caloric diet (HFD) feeding and may also be contributed by chronic stress; however, the neural basis underlying stress-related diet-induced obesity remains unknown. Corticotropin-releasing hormone (CRH) neurons in the paraventricular hypothalamus (PVH), a known body weight-regulating region, represent one key group of stress-responsive neurons. Here, we found that HFD feeding blunted PVH CRH neuron response to nutritional challenges as well as stress stimuli and dexamethasone, which normally produce rapid activation and inhibition on these neurons, respectively. We generated mouse models with the activity of these neurons clamped at high or low levels, both of which showed HFD-mimicking, blunted PVH CRH neuron responsiveness. Strikingly, both models developed rapid HFD-induced obesity, associated with HFD-mimicking, reduced diurnal rhythmicity in feeding and energy expenditure. Thus, blunted responsiveness of PVH CRH neurons, but not their absolute activity levels, underlies HFD-induced obesity and may also contribute to stress-induced obesity.

Keywords CRH; HFD; obesity; PVH; stress

Subject Categories Metabolism; Neuroscience

DOI 10.15252/embr.201949210 | Received 3 September 2019 | Revised 19 April 2020 | Accepted 24 April 2020 | Published online 27 May 2020

EMBO Reports (2020) 21: e49210

Introduction

The current obesity epidemic coincides with social and economic improvements. Susceptibility to obesity development is thus speculated to be caused by a combination of genetics and environmental

changes, including easy access to high-fat high-caloric diets (HFD), and stresses imposed by increasing socioeconomic pressure [1–4]. Specifically, HFD feeding is associated with disrupted diurnal rhythms in feeding and metabolism, and time-scheduled feeding alleviates the obesity and associated metabolic syndromes by HFD [5], suggesting an important contribution of disrupted diurnal rhythms to diet-induced obesity (DIO). Recent studies have also suggested a potential role for stress in worsening DIO [6–9]. Despite intense research, the cellular mechanism in the brain underlying HFD feeding and its potential interaction with stress in obesity development remains elusive.

Corticotropin-releasing hormone-expressing (CRH) neurons, widely distributed in the brain [10], are known to be the major subset of brain neurons that orchestrate behavioral and hormonal responses to stress [11]. Anatomically, hypothalamic CRH neurons serve as a link between metabolism regulation and stress responses. These neurons are known to elicit neuroendocrine responses through the autonomic nervous system and hypothalamus–pituitary–adrenal axis (HPA) [12,13], although emerging studies suggest a role for PVH CRH neurons in mediating stress behaviors [14,15]. In addition to stress responses, these neurons are shown to be important for diet preference [16], suggesting potential relevance to obesity development. Pathologically, uncontrolled glucocorticoid levels are known to be associated with hyperphagia, insulin resistance, obesity, and diabetes, as observed in human Cushing’s diseases and leptin-deficient *ob/ob* mouse models [17,18]. However, other studies have also suggested that PVH CRH neurons play a minimal role in feeding or obesity development [15,19,20]. Thus, the relevance of CRH function to DIO is not yet clear.

High-fat high-caloric diet feeding has been shown to blunt diurnal rhythms [5,21,22]. Specifically, HFD reduces HPA axis activity and diurnal corticosterone rhythms in mice [23–25], and a disrupted corticosterone diurnal pattern is also present in obese *ob/ob* and

1 Guangdong Laboratory of Lingnan Modern Agriculture, Guangdong Province Key Laboratory of Animal Nutritional Regulation and National Engineering Research Center for Breeding Swine Industry, College of Animal Science, South China Agricultural University, Guangzhou, China

2 Brown Foundation Institute of Molecular Medicine of McGovern Medical School, University of Texas Health Science Center at Houston, Houston, TX, USA

3 Department of Integrative Physiology and Pharmacology, McGovern Medical School, Houston, TX, USA

4 Graduate Program in Neuroscience of MD Anderson Cancer Center UTHealth Graduate School of Biomedical Sciences, University of Texas Health Science Center at Houston, Houston, TX, USA

5 Department of Neuroscience, Baylor College of Medicine, Houston, TX, USA

6 The Cain Foundation Laboratories, Jan and Dan Duncan Neurological Research Institute at Texas Children’s Hospital, Houston, TX, USA

7 Children’s Nutrition Research Center, Department of Pediatrics, Baylor College of Medicine, Houston, TX, USA

8 Department of Neuroscience, Baylor College of Medicine, Jan and Dan Duncan Neurological Research Institute, Texas Children’s Hospital, Houston, TX, USA

9 Department of Neurobiology and Anatomy, McGovern Medical School at the University of Texas Health Science Center at Houston, Houston, TX, USA

*Corresponding authors. Tel: +86 20 85281269; E-mail: qyjiang@scau.edu.cn

**Corresponding author. Tel: +1 713 500 3453; E-mail: qingchun.tong@uth.tmc.edu

db/db mouse models [26], pointing to a potential importance of PVH CRH neuron activity changes in response to HFD feeding and in obesity development. In this study, we therefore aim to test the hypothesis that HFD-induced defective responsiveness of PVH CRH neurons contributes to DIO. Our results show that HFD disrupts the responsiveness of PVH CRH neurons and our animal models with PVH CRH neurons chronically clamped at high or low levels both exhibit disrupted neuron responsiveness, susceptibility to DIO, and defective diurnal rhythms in metabolism, thus revealing blunted responsiveness of these neurons as a novel contributor to DIO.

Results and Discussion

Paraventricular hypothalamus neurons are known to be activated during nutritional challenges in switching from fasting to refeeding [27,28]. While PVH neurons exhibit little *c-Fos* expression with *ad libitum* fed conditions either on chow or HFD (Fig EV1A), a subset of PVH neurons in chow-fed control mice exhibited *c-Fos* expression when switching from fast to refeed conditions (Fig 1A and B). In contrast, with 4-week HFD feeding, the number of *c-Fos*-expressing neurons was dramatically reduced (Fig 1A and B). We used CRH-Cre::Ai9 reporter mice to specifically examine *c-Fos* expression in CRH neurons and found that HFD feeding largely eliminated *c-Fos* expression in PVH CRH neurons (Fig 1A and C), suggesting that HFD feeding greatly reduced the response of PVH CRH neurons to a switch from fasting to refeed, a nutritional challenge frequently experienced in mice. As expected, mice during the 4-week HFD feeding exhibited increased energy intake, reduced energy expenditure, and increased body weight. In addition, these mice also reduced their diurnal rhythmicity in both feeding (Fig 1D and E) and energy expenditure (Fig 1F and G), supporting earlier findings on significant contributions of diminished diurnal feeding and energy expenditure patterns to DIO [5].

To examine whether HFD disrupts PVH CRH neuron responses to acute stress stimuli, we recorded the activity of these neurons in freely behaving animals with the fiber photometry method [29,30]. For this, we delivered AAV-Flex-GCaMP6m to the PVH of CRH-Cre mice with implanted optic fibers targeting the PVH (Fig EV1B).

Consistent with the role of PVH CRH neurons in stress responses, applications of stressors, i.e., water spray, induced a robust increase in PVH CRH neuron activity, which lasted 2–3 s (Fig 1H and J). The mice were then switched to HFD and maintained on the same diet for 4 weeks before a new round of fiber photometry measurement with the same water spray stimulus. Those PVH CRH neurons of the same mice greatly diminished their responses to water spray (Fig 1I and J). To examine whether the diminished response is specific to stress-induced activation, we also applied dexamethasone (Dex), an analog of corticosterone (Cort) known to inhibit PVH CRH neurons. While saline administration failed to produce changes (Fig EV1C), Dex inhibited PVH CRH neuron activity within minutes (Fig 1K and M), which is likely mediated by its membrane receptors [31]. This effect was greatly diminished in PVH CRH neurons 4 weeks after HFD feeding (Fig 1L and M). These results demonstrate that HFD feeding reduces PVH CRH neuron responsiveness.

To test whether dampening PVH CRH responsiveness contributes to DIO, we aimed to generate animal models with disrupted responsiveness in PVH CRH neurons by clamping the neuron activity at high levels. The expression of *NachBac*, a sodium channel from bacteria, is known to increase baseline neuronal activity [32,33]. We therefore delivered AAV-EF1a-Flex-EGFP-P2A-m*NachBac* to the PVH of CRH-Cre mice. We recorded CRH neurons with *NachBac* expression in one side of the PVH, compared to those recorded in the other side with control neurons of the same animal 4 weeks after viral delivery (Fig 2A). Compared to controls, which showed spontaneous tonic firing around -50 mV, spontaneous burst firing and long-lasting plateau depolarization were recorded at more negative membrane potential (-65 mV) from *NachBac* neurons (Fig 2B). This more negative membrane potential may result from a compensatory response to avoid overexcitation. With a step-wise voltage clamp protocol to evoke Na^+ channel activation, compared to the -40 mV threshold found in control cells (Fig EV2A), *NachBac* channels were activated at -50 mV, with much slower inactivation than the endogenous Na^+ channels (Fig EV2B). In total, while 12 out of 15 recorded *NachBac* neurons (80%) showed spontaneous firing despite their more negative membrane potentials than that in controls cells, in which only six of 10 control cells (60%) exhibited spontaneous firing (Fig 2C). The higher percentage of spontaneous firing in *NachBac*-expressing neurons suggest they are more active

Figure 1. HFD blunted PVH CRH neuron responsiveness.

- A–C CRH-Cre::Ai9 reporter male mice fed on chow or 4 weeks on HFD were used to examine *c-Fos* expression in the PVH in 24 h fasting or refeed after 24 h fasting. (A) Representative images showing CRH neurons (red in the first column), *c-Fos* expression (green in the second column), merged images of red and green (the third column), and the amplified pictures for the boxed areas in the merged images (the fourth column). The experimental conditions for each group (fasting versus refeed, chow versus HFD) are labeled on the left. Scale bar = 200 μm . (B, C) Comparison of average neuron numbers from cell counting on total number of *c-Fos*-positive neurons in the PVH (B, $**P = 0.0032$: chow fasting versus chow refeed and $*P = 0.023$, HFD fasting versus HFD refeed) and total number of *c-Fos*-positive CRH neurons (C, $**P < 0.0001$: chow fasting versus chow refeed and $P = 0.7158$: HFD fasting versus HFD refeed), $n = 3–4$ each, data presented as mean \pm SEM, two-way ANOVA tests.
- D–G Effects of HFD feeding on diurnal rhythmicity in feeding (D and E) and energy expenditure (F and G). The measurement was collected with male mice fed chow or after 4-week HFD feeding, $n = 6$ each, data presented as mean \pm SEM, $**P = 0.0066$ in E and $**P = 0.00007$ in G, unpaired Student's *t*-tests.
- H–M CRH-Cre mice received delivery of AAV-Flex-GCaMP6m viral vectors to bilateral PVH and optic fiber implantation targeting PVH neurons and were used for *in vivo* live recording. (H, I) Representative traces showing recordings of activity changes in CRH neuron in response to stressor (water spray) in chow-fed controls (H) and 4 weeks after HFD (I), (J) Comparison of average responses in the two conditions, $n = 4$ each, $**P = 0.0006$, paired Student's *t*-test. (K, L) Representative traces showing recordings of activity changes in CRH neurons in response to dexamethasone (Dex) injections in chow-fed controls (K) and after 4 weeks on HFD (L). (M) Comparison of average responses in the two conditions, $n = 4$ each, data presented as mean \pm SEM, $**P = 0.0012$, paired Student's *t*-tests.

Data information: 3V: the third ventricle; downward arrows indicating onset of stimuli or Dex injections.

Source data are available online for this figure.

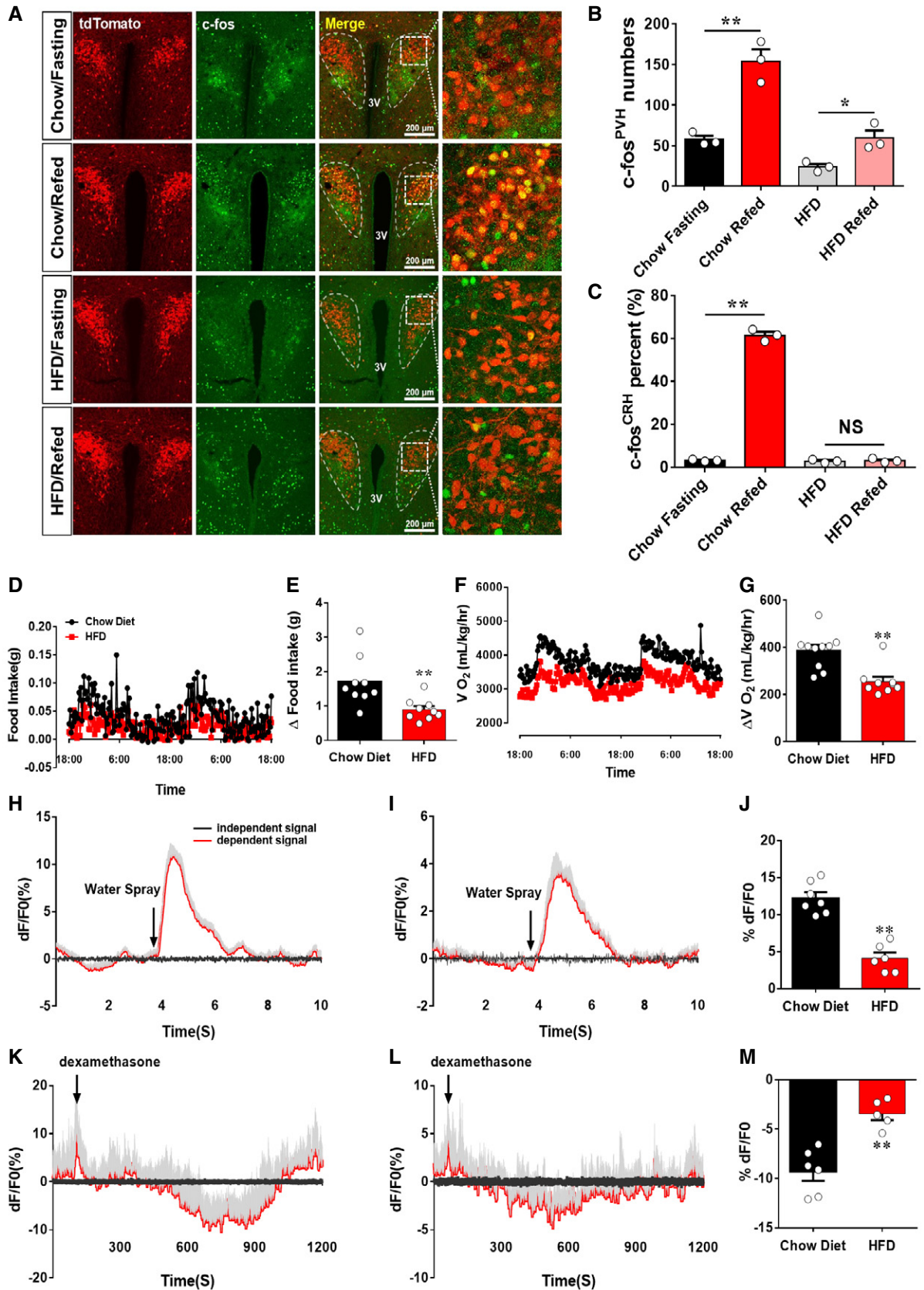


Figure 1.

than control neurons. To further confirm that NachBac-expressing neurons exhibit a high level of activity *in vivo*, we examined c-Fos expression in the PVH in response to a switch from fasting to refeeding. As expected, in control CRH-Cre mice with AAV-Flex-GFP injections to bilateral PVH, c-Fos was induced in the PVH (Fig 2D and E), especially in PVH GFP-labeled CRH neurons (Fig 2F). In CRH-Cre mice with AAV-EF1a-Flex-EGFP-P2A-mNachBac injection to bilateral PVH, a much greater number of PVH neurons exhibited c-Fos expression both at fasting and refeed conditions (Fig 2D and E). Interestingly, in contrast to control CRH neurons, switching mice from fasting to refeeding failed to induce further c-Fos expression in NachBac-expressing neurons (Fig 2D and F), suggesting that NachBac expression effectively clamps CRH neuron activity as high levels, disrupting the ability of these neurons in responding to nutritional challenges.

In addition, we also examined the response of NachBac-expressed PVH CRH neurons to acute stressors and Dex. Toward this, we delivered AAV-Flex-GCaMP6m and AAV-EF1a-Flex-EGFP-P2A-mNachBac simultaneously to bilateral PVH of CRH-Cre mice for fiber photometry recording (Appendix Fig S1A). In contrast to rapid and strong activation on CRH neurons (Fig 1H), water spray failed to induce obvious changes in NachBac-expressing CRH neurons (Fig 2G and H). A similar observation was also made in response to Dex (Fig 2I and J). Notably, PVH CRH neurons with NachBac expression were greatly inhibited by exposure to isoflurane, an anesthetic with potent inhibitory action on neurons (Appendix Fig S1B), ruling out the possibility that failure in detecting CRH neuron response is an artifact of experimental defects. To examine the possibility that co-expression of additional fluorescent protein (e.g., GFP in the NachBac vector) might interfere with GCaMP6m measurements, we compared GCaMP6m measurements among three groups of CRH-Cre mice with delivery of AAV-Flex-GCaMP6m alone (Appendix Fig S1C), AAV-Flex-GCaMP6m plus AAV-Flex-GFP (Appendix Fig S1D), or AAV-Flex-GCaMP6m plus AAV-Flex-mCherry (Appendix Fig S1E). No difference was observed

among the three groups in the GCaMP6m signal in response to water spray (Appendix Fig S1F), suggesting that presence of other fluorescence (green or red) has no interference on measurements of GCaMP6m signals. Taking together, NachBac expression effectively increases the activity level and blunts the responsiveness of PVH CRH neurons.

Paraventricular hypothalamus CRH expression is known to exhibit a diurnal pattern, with a higher level at night periods [34], suggesting the activity of these neurons in a diurnal pattern. In addition to direct projections to other brain regions, PVH CRH neurons are known to regulate the HPA axis. To further test whether NachBac expression disrupts diurnal neuron activity pattern, we measured corticosterone (cort) levels across 24 h and found that NachBac mice exhibited much greater levels during night times, compared to controls (Fig EV2C). As cort is a remote indicator for CRH neuron activity and especially its level is controlled by complex feedback regulation through its own control at both CRH and pituitary levels, the diurnal pattern of cort may not necessarily reflect PVH CRH neuron activity pattern. Supporting this, mice with PVH-specific deletion of glucocorticoid receptor, known to inhibit CRH expression, show disrupted diurnal patterns in adrenocorticotropic hormone (ACTH) and exhibit heightened diurnal changes in cort levels [35]. We therefore used CRH expression level as a proxy for CRH neuron activity. Notably, CRH immunostaining showed an increased CRH accumulation in the median eminence (ME), where CRH neuron fibers are located (Fig EV3D). Consistent with the fact that CRH is normally transported to terminals, CRH immunostaining failed to show clear immunoreactive structures in PVH CRH neurons during both morning and night periods in controls; however, NachBac mice showed abundant CRH-immunoreactive soma and fibers in the PVH at both day and night periods (Fig EV2E). These data, although on their own, cannot approve, nevertheless support, that NachBac expression increases PVH CRH neuron activity and disrupts diurnal patterns of activity.

Figure 2. Clamping PVH CRH neuron activity at high levels disrupted neuron responsiveness.

- A–C CRH-Cre male mice received stereotaxic delivery of AAV-EF1a-Flex-EGFP-P2A-mNachBac vectors at 7–8 weeks of age and recordings were made at least 4 weeks after viral delivery on neurons with NachBac (one side) or control neurons (contralateral side) of the same animal (A); typical action potentials (APs) in controls (B, top panel) and typical NachBac-mediated APs showing lower threshold and long duration (B, bottom, the inset highlighting the long duration) in NachBac mice; and the distribution of the membrane potential and firing cells in the two groups (C, ratios in the bracket denoting neuron number out of total number recorded with the indicated behavior).
- D–F CRH-Cre male mice were injected with either AAV-Flex-GFP or AAV-EF1a-Flex-EGFP-P2A-mNachBac to examine c-Fos expression in the PVH in 24 h fasting or refeed after fasting. (D) Representative images showing CRH neurons expressing GFP or NachBac (GFP in the top two rows and NachBac in the bottom two rows of the first column), c-Fos expression (red in the second column), merged images of red and green (the third column), and the amplified pictures for the boxed areas in the merged images (the fourth column). The experimental conditions for each group (fasting versus refeed) are labeled on the left. (E, F) Comparison of average neuron numbers from cell counting on total number of c-Fos-positive neurons in the PVH (E, $**P < 0.0001$: fasting versus refeed; $**P = 0.0026$: fasting versus fasting/NachBac; $**P < 0.0001$: fasting/NachBac versus refeed/NachBac) and total number of c-Fos-positive CRH neurons (F, $**P < 0.0001$: fasting versus refeed; $**P < 0.0001$: fasting versus fasting/NachBac; $P = 0.3423$: fasting/NachBac versus refeed/NachBac), $n = 3–4$ each, data presented as mean \pm SEM, two-way ANOVA tests.
- G–J CRH-Cre male mice received stereotaxic delivery of a mixture of AAV-Flex-GCaMP6m and AAV-EF1a-Flex-EGFP-P2A-mNachBac vectors at 7–8 weeks of age with optic fiber implantation targeting PVH neurons. (G, H) Representative traces showing typical responses of PVH CRH neurons to water spray (arrows) in NachBac mice (G) and comparison of responsiveness to water spray between NachBac and control mice (H). (I, J) Representative traces showing typical responses of PVH CRH neurons to water spray (arrows) in NachBac mice (I) and comparison of responsiveness to water spray between NachBac and control mice (J). Gray traces showed Ca^{2+} -independent signal for system stability, and red ones showed Ca^{2+} -dependent signals for neuron activity, $N = 5–7$ each, males, data presented as mean \pm SEM, $**P < 0.0001$ in both (H and J), unpaired Student's *t*-tests.

Data information: All mice were fed chow unless otherwise noted. 3V: the third ventricle; downward arrows indicating onset of stimuli or Dex injections. Scale bar = 200 μ m.

Source data are available online for this figure.

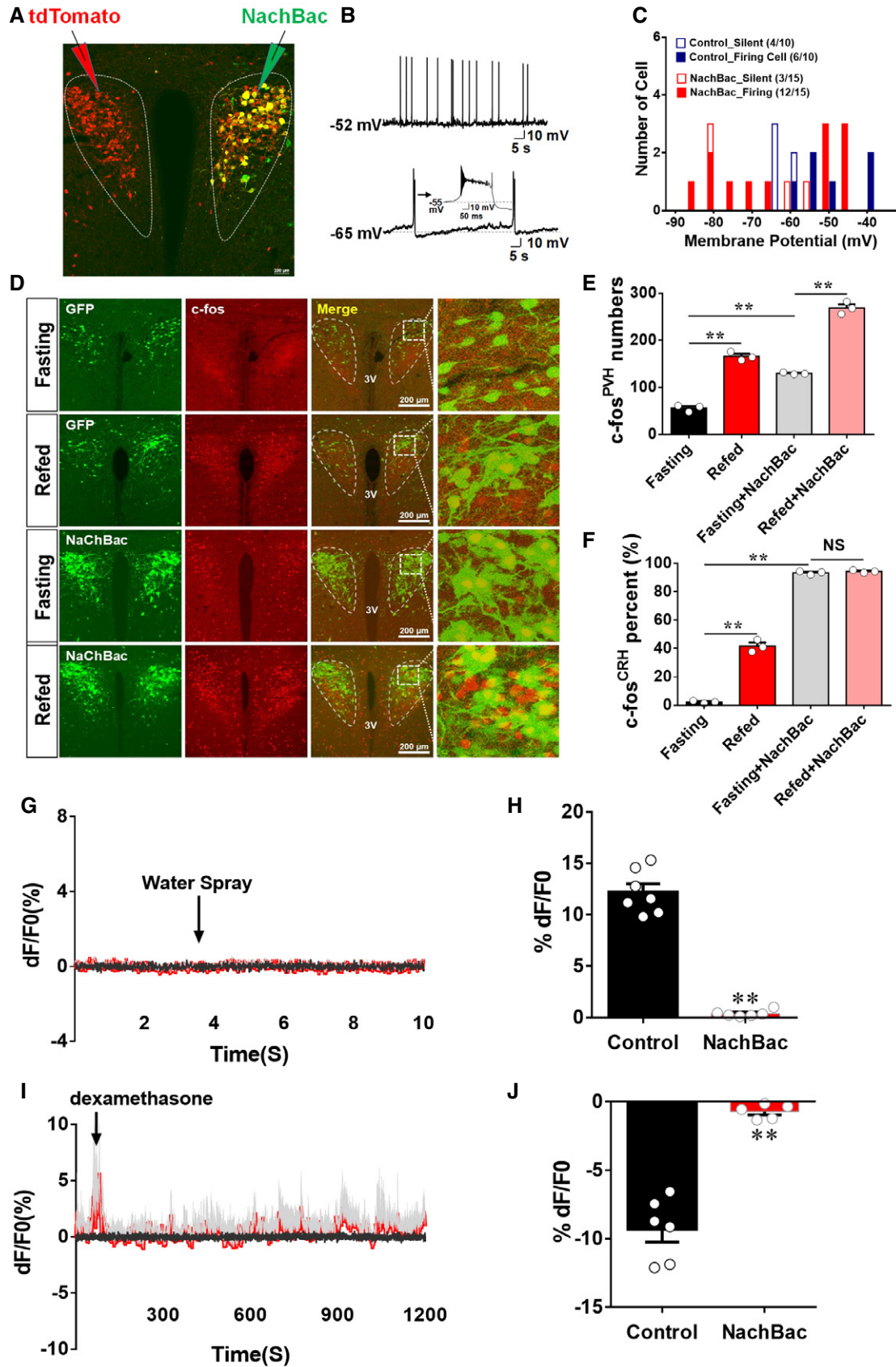


Figure 2.

We then used mice with NachBac vector injections to bilateral PVH of CRH-Cre mice to examine the effect on body weight. When fed chow, NachBac mice gained a slightly but significant more body weight than controls (Fig 3A). However, after exposure to HFD, these mice gained rapid body weight and were 10 g heavier than controls 4 weeks after HFD diet switch (Fig 3A). The observed body weight gain was associated with increased fat mass (Fig 3B), but no changes in lean mass (Fig 3C), suggesting obesity development. When measured at 7 weeks after viral delivery but before HFD switch, these mice exhibited lower energy expenditure (Fig 3D and E) and greater feeding levels (Fig 3G and H). Interestingly, when the difference between day and night periods was compared, NachBac mice showed much less difference in either energy expenditure (Fig 3F) or feeding (Fig 3I), suggesting reduced rhythmicity in both, which is reminiscent to the dampening effect on diurnal rhythmicity by HFD feeding [5]. When comparison between the two groups during light and dark periods was performed, we found that NachBac mice ate more food but spent less energy, especially during light periods (Fig EV3A–D), suggesting an increased feeding efficiency. A similar reduction in activity level in NachBac mice was also observed (Fig EV3E–I). Weekly glucose levels trended to increase on chow but were significantly elevated in HFD-fed conditions (Fig EV3J), likely due to a secondary effect of obesity development. In addition, NachBac mice exhibited an increased anxiety level in our behavioral tests (Appendix Fig S2). These data collectively demonstrate that clamping PVH CRH neuron activity at high levels diminishes the responsiveness of these neurons and leads to DIO.

The aforementioned results suggest that NachBac expression diminished PVH CRH responsiveness while increased the activity level of these neurons. To ascertain the role of diminished responsiveness in DIO and rule out a potential direct role from an increased neuron activity level, we aimed to generate a new mouse model with disrupted PVH CRH neuron responsiveness through clamping neuron activity at low levels. Towards this end, we used a mutated form of the Kir2.1 channel, which has previously used to reduce neuron activity [32]. We delivered either AAV-Flex-GFP vectors to one side as control or AAV-EF1a-DIO-Kir2.1-P2A-dTomato vectors to the other side of the PVH of CRH-Cre mice for recording experiments (Fig 4A). Compared to controls, Kir2.1 expression reduced resting membrane potential (Fig 4B and C) and significantly increased the size of minimum currents required to be injected to elicit action potential, i.e., rheobase (Fig EV4A–C), suggesting that expression of Kir2.1 effectively reduces the PVH neuron activity.

We next examined the effect of Kir2.1 expression on c-Fos induction in response to switch from fasting to refeeding. We delivered AAV-EF1a-DIO-Kir2.1-P2A-dTomato vectors to one side of the PVH of CRH-Cre mice (Fig 4D), which allows to effectively examine the effect of Kir2.1 on c-Fos expression by using the other side of PVH with no Kir2.1 expression within the same brain as control conditions. Compared to controls, Kir2.1 expression in PVH CRH neurons significantly reduced the number of c-Fos positive neurons in the PVH during fast-refeeding transitions (Fig 4D and E). When counting PVH CRH neurons with c-Fos expression, we found that while the control side with mCherry expression showed a great number of PVH CRH neurons with c-Fos expression, few of these neurons with Kir2.1 expression was found to express c-Fos during the fast-

refeeding switch (Fig 4D and F), suggesting that expression of Kir2.1 effectively clamped PVH CRH neuron activity at low levels and disrupted the ability of these neurons in responding to nutritional challenges during fast-refeeding transitions.

We further examined the impact of Kir2.1 expression on PVH CRH neuron response to acute stress and hormonal action. In CRH-Cre mice with co-injections of AAV-Flex-GCaMP6m and AAV-EF1a-DIO-Kir2.1-P2A-dTomato (Appendix Fig S3A), in contrast to controls, water spray (Fig 4G and H) or Dex administration (Fig 4I and J) failed to induce changes in the activity of CRH neurons. To verify that the failure in PVH CRH neuron response is not due to an experimental defect, we performed similar isoflurane inhalation as previously described and found that isoflurane was effective in reducing the activity of these neurons (Appendix Fig S3B). Thus, clamping PVH neuron activity at low levels with Kir2.1 expression is sufficient to blunt the responsiveness of these neurons, in a similar fashion to HFD feeding.

We also measure the HPX axis to confirm the effect of Kir2.1 inhibition. Compared to a nature diurnal pattern of cort, Kir2.1 mice exhibited a flat pattern across 24 h (Fig EV4D), suggesting chronic inhibition of PVH CRH neurons is sufficient to diminish diurnal cort pattern. We then used CRH-Cre::Ai9 mice (Fig EV4E and G) and CRH-Cre mice with one side injection of Kir2.1 vectors (Fig EV4F and H) to examine the effect of Kir2.1 inhibition on CRH expression. While control mice exhibited even CRH immunoreactivity between the two sides of ME, Kir2.1 mice showed much less CRH immunoreactivity in the side with more Kir2.1 expression (Fig EV4H), demonstrating inhibition of CRH expression by Kir2.1.

We then delivered the Kir2.1 vector to bilateral PVH of CRH1-Cre mice for body weight studies. While Kir2.1-expressing mice showed no difference in body weight on chow diet, they gained more body weight once switched to HFD (Fig 5A). The increased body weight is associated with increased fat mass (Fig 5B) but no changes in lean mass (Fig 5C), suggestive of obesity development. When measured between 7 and 8 weeks after viral delivery, energy expenditure was reduced (Fig 5D and E) and, importantly, the difference between night and day in energy expenditure was reduced in mice with Kir2.1 expression (Fig 5F). Food intake was increased (Fig 5G and H), and the difference between night and day in feeding was also reduced in mice with Kir2.1 expression (Fig 5I). When comparison during light and dark periods was performed, we found that Kir2.1 mice ate more food but spent less energy, especially during light periods (Fig EV5A–D), suggesting an increased feeding efficiency. A similar reduction in activity level in NachBac mice was also observed (Fig EV5E–I). These data demonstrate that Kir2.1 expression reduces PVH CRH neuron activity, disrupts the responsiveness of these neurons, and leads to DIO. Notably, despite no body weight difference when fed chow, these mice exhibited lower blood glucose levels, but rapidly increased their glucose levels to a similar level of controls after exposure to HFD, likely due to their development of obesity (Fig EV5J). Collectively, these results suggest that PVH CRH neuron activity clamped at either high or low levels both blunted responsiveness of these neurons and induced DIO. Thus, disrupted responsiveness of PVH CRH neurons, but not their absolute activity levels, predisposes to DIO.

In this study, we found that HFD feeding blunted the response of PVH CRH neurons to nutritional challenges, acute stressors, and hormonal action. To test whether the blunted responsiveness

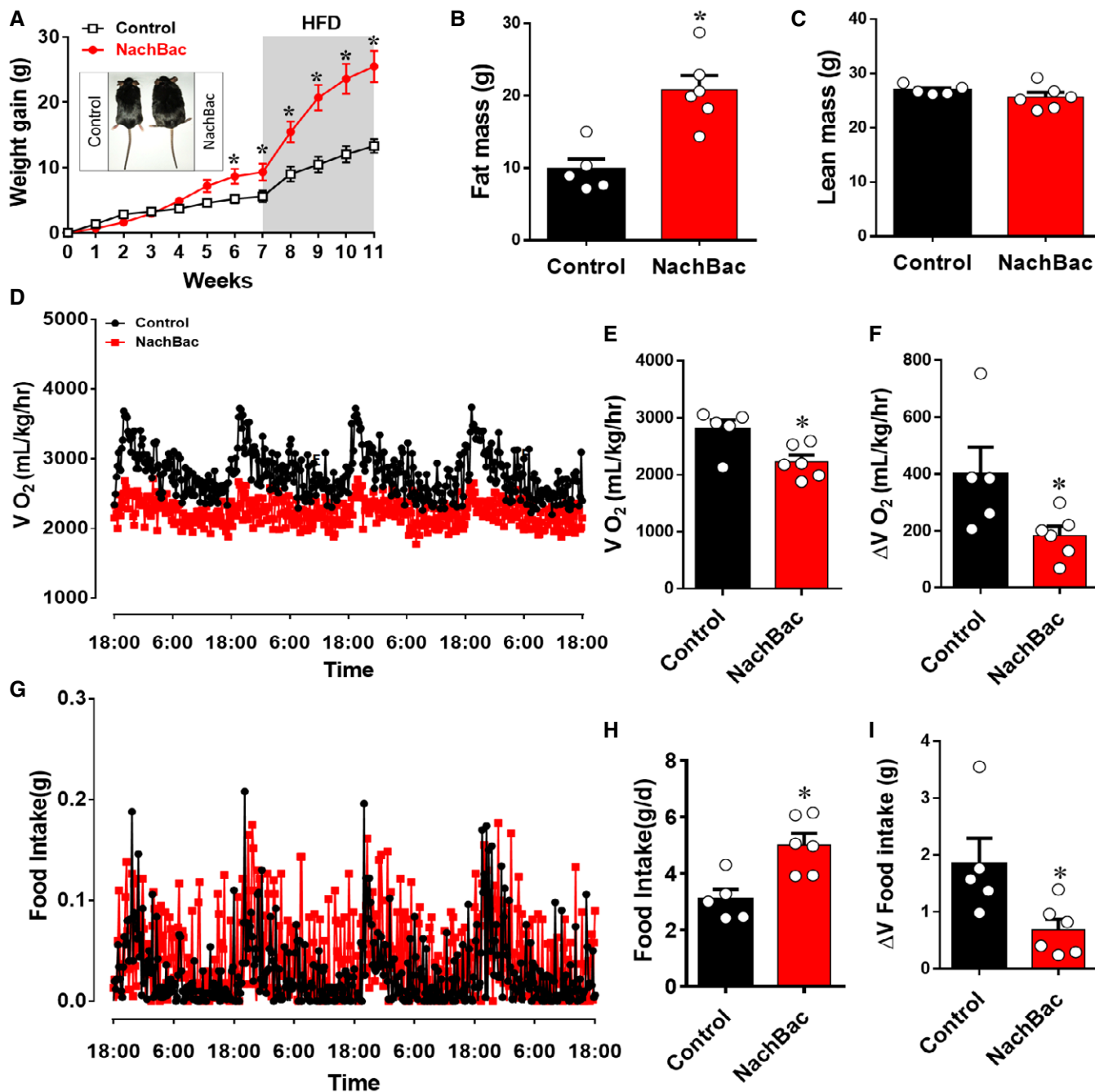


Figure 3. Clamping PVH CRH neuron activity at high levels causes rapid diet-induced obesity.

A–I CRH-Cre male mice received stereotaxic delivery of AAV-EF1a-Flex-EGFP-P2A-mNachBac or control GFP vectors at 7–8 weeks of age and were maintained on chow diet for 7 weeks before switching to HFD. Weekly body weight gain after viral delivery (A), and measurements of fat mass (B) and lean mass (C) at 11 weeks after viral delivery. (D–F) Measurements of energy expenditure during the 7th week after viral delivery. Comparison of real-time O_2 consumption traces during the 4-day measurement period (D), of average O_2 consumption between the two groups (E), and of the difference between day and night periods between the two groups (F). (G–I) Measurements of feeding during the 7th week after viral delivery. Comparison of real-time feeding traces during the 4-day measurement period (G), of average food intake between the two groups (H), and of the difference in food intake between day and night periods between the two groups (I). $n = 5–6$ each, * $P < 0.0001$ in A, * $P = 0.0019$ in B, $P = 0.2316$ in C, * $P = 0.0196$ in E, * $P = 0.0466$ in F, * $P = 0.0062$ in H, and * $P = 0.0298$ in I, unpaired Student’s t-tests. All data presented as mean \pm SEM.

Source data are available online for this figure.

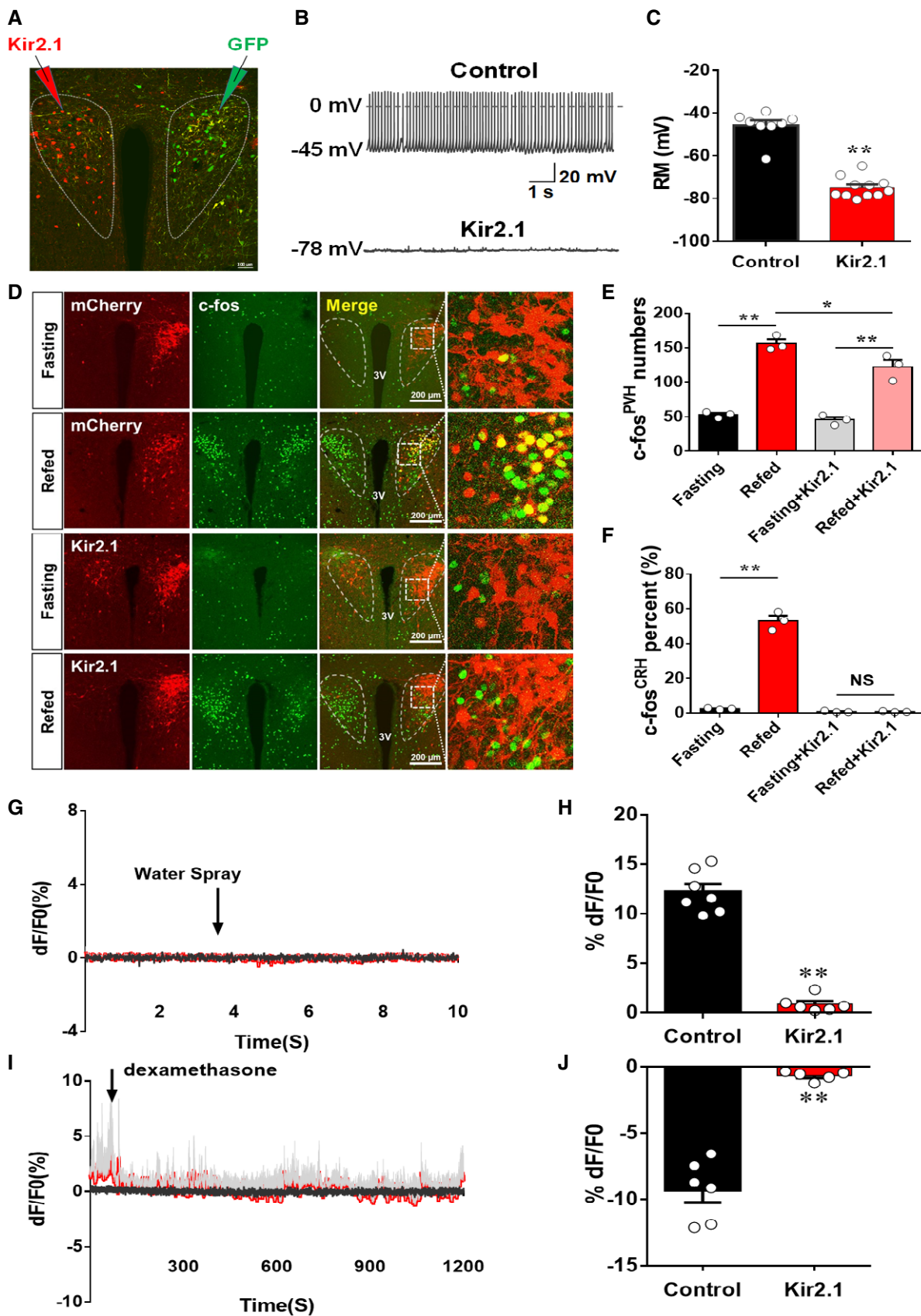


Figure 4.

Figure 4. Clamping PVH CRH neuron activity at low levels disrupted neuron responsiveness.

- A–C CRH-Cre male mice received stereotaxic delivery of AAV-EF1a-DIO-Kir2.1-P2A-dTomato vectors and AAV-Flex-GFP at 7–8 weeks of age, and recording was made at least 4 weeks after viral delivery on neurons with Kir2.1 (one side) or control GFP neurons (contralateral side) of the same animal (A); typical spontaneous neuron activity recorded in GFP controls (B, top panel) and Kir2.1 neurons (B, bottom); and comparison in resting membrane potentials between the two groups (C, $**P < 0.0001$, unpaired Student's *t*-test).
- D–F CRH-Cre male mice were injected with either AAV-Flex-mCherry or AAV-EF1a-DIO-Kir2.1-P2A-dTomato to examine c-Fos expression in the PVH in 24 h fasting or refed after fasting. (D) Representative images showing CRH neurons expressing mCherry or Kir2.1 (mCherry in the top two rows and Kir2.1 in the bottom two rows of the second column), c-Fos expression (green in the first column), merged images of red and green (the third column), and the amplified pictures for the boxed areas in the merged images (the fourth column). The experimental conditions for each group (fasting versus refed) are labeled on the left. (E, F) Comparison of average neuron numbers from cell counting on total number of c-Fos-positive neurons in the PVH (E, $**P = 0.0001$: fasting versus refed; $*P = 0.0497$: refed versus refed/Kir2.1; $**P = 0.0025$: fasting/Kir2.1 versus refed Kir2.1) and total number of c-Fos-positive CRH neurons (F, $**P < 0.0001$: fasting versus refed; $P = 0.9586$: fasting/Kir2.1 versus refed/Kir2.1), $n = 3–4$ each, two-way ANOVA tests. All data presented as mean \pm SEM.
- G–J CRH-Cre male mice received stereotaxic delivery of a mixture of AAV-Flex-GCaMP6m and AAV-EF1a-DIO-Kir2.1-P2A-dTomato vectors at 7–8 weeks of age with optic fiber implantation targeting PVH neurons. (G–H) Representative traces showing typical responses of PVH CRH neurons to water spay (arrows) in Kir2.1 mice (G) and comparison of responsiveness to water spray between Kir2.1 and control mice (H). (I, J) Representative traces showing typical responses of PVH CRH neurons to water spay (arrows) in Kir2.1 mice (I) and comparison of responsiveness to water spray between Kir2.1 and control mice (J). Gray traces showed Ca^{2+} -independent signal for system stability, and red ones showed Ca^{2+} -dependent signals for neuron activity, $N = 5$ each, males, data presented as mean \pm SEM, $**P < 0.0001$ in both (H and J), unpaired Student's *t*-tests.

Data information: All mice were fed chow unless otherwise noted. 3V: the third ventricle; downward arrows indicating onset of stimuli or Dex injections. Scale bar = 200 μ m.

Source data are available online for this figure.

mediates DIO, we created two complementary animal models with PVH CRH neuron activity clamped at either high or low levels, both confirmed to exhibit blunted responsiveness, mimicking the effect of HFD feeding. Interestingly, despite differences in body weight and glucose homeostasis on chow, both models developed rapid DIO. These results demonstrate that it is the responsiveness of PVH CRH neurons, but not their absolute activity level, dictates the susceptibility to DIO, thus providing a novel insight on the mechanism underlying DIO. This novel mechanism has important implications to prevalent investigations focusing on the role of neuron activity levels in the regulation of feeding and obesity development.

One potential mechanism for HFD to diminish neuron responsiveness may lie in alterations in synaptic neurotransmission from upstream neurons, given that HFD is known to cause rapid changes in synaptic currents on hypothalamic neurons [36–38]. One upstream site might be arcuate neurons, which are known to provide direct synaptic inputs to PVH neurons and respond to ambient signals including those induced by HFD feeding [39]. Disrupted neuron responsiveness may also lie in the changes within PVH CRH neurons induced by HFD diet as these neurons also exhibited reduced responses to Dex, a hormone that presumably acts directly on these neurons. The expression of either NachBac or Kir2.1 greatly blunted the responsiveness, suggesting that the action of NachBac and Kir2.1, which likely lock the neuron activity at respective elevated or reduced levels, may override the action induced by stressors and hormones. Notably, mice with NachBac expression exhibited a significant increase in body weight on chow, suggesting a sufficiency of chronic activation of PVH CRH neurons in causing a HFD-mimicking effect. No body weight difference observed in Kir2.1 mice on chow may be due to a beneficial effect of reducing PVH CRH neuron activity, as evidenced from improved glucose homeostasis in these mice, which was quickly reversed on HFD. The greater susceptibility of these mice to DIO demonstrates that appropriate responses of these neurons to HFD feeding are required to mount balanced body weight regulation on HFD feeding.

High-fat high-caloric diet-induced disruption in the responsiveness of PVH CRH neurons has important implications. As PVH CRH

neuron activity regulates the HPA axis, our findings are supported by previous studies showing that HFD blunts the HPA axis and alters diurnal rhythms of cort [23,24,40]. The reduced responsiveness of PVH CRH neurons may underlie the effect of chronic stress on exacerbating HFD-induced obesity. Chronic stress induces a sustained increase in the activity of PVH CRH neurons [41], which may mimic the effect induced by NachBac in clamping the neuron activity at high levels. Thus, disrupted neuron responsiveness may explain obesity development induced by chronic stressors (e.g., social stress) [42,43] and synergistic effects between chronic stress and HFD on obesity development [6–9]. Given the socioeconomic stress faced by humans is chronic in nature, and a positive correlation between cort levels and low socioeconomic status [44], our results support that chronic stress contributes significantly to obesity development, especially in the current HFD environment.

The PVH CRH neuron activity pattern is orchestrated by dynamic changes in synaptic inputs and hormonal action [13]. Thus, disruption in the response of these neurons to stressors and hormonal action may impact long-term activity patterns of these neurons. It is known that both CRH and cort levels exhibit a diurnal pattern in mice [34,45], indicating that PVH CRH neurons may exhibit a diurnal pattern of activity. Thus, although remains to be determined, HFD feeding, and NachBac or Kir2.1 expression may disrupt diurnal patterns of PVH CRH neurons. Given the reduced diurnal rhythmicity in feeding and energy expenditure as a common feature in all animal models presented in this study, it is likely that loss of diurnal metabolism in DIO may be contributed significantly by disrupted diurnal activity pattern of PVH CRH neurons owing to loss of responsiveness. As scheduled feeding is known to improve metabolism and diurnal rhythms [5], it would be interesting in future studies to examine whether HFD-induced disruption in responsiveness of PVH CRH neurons can be reversed by scheduled feeding. In summary, our current findings reveal a novel mechanism underlying DIO in which HFD feeding diminishes responsiveness of PVH CRH neurons, thereby affecting diurnal rhythms in feeding and metabolism and leading to obesity development, and that PVH CRH

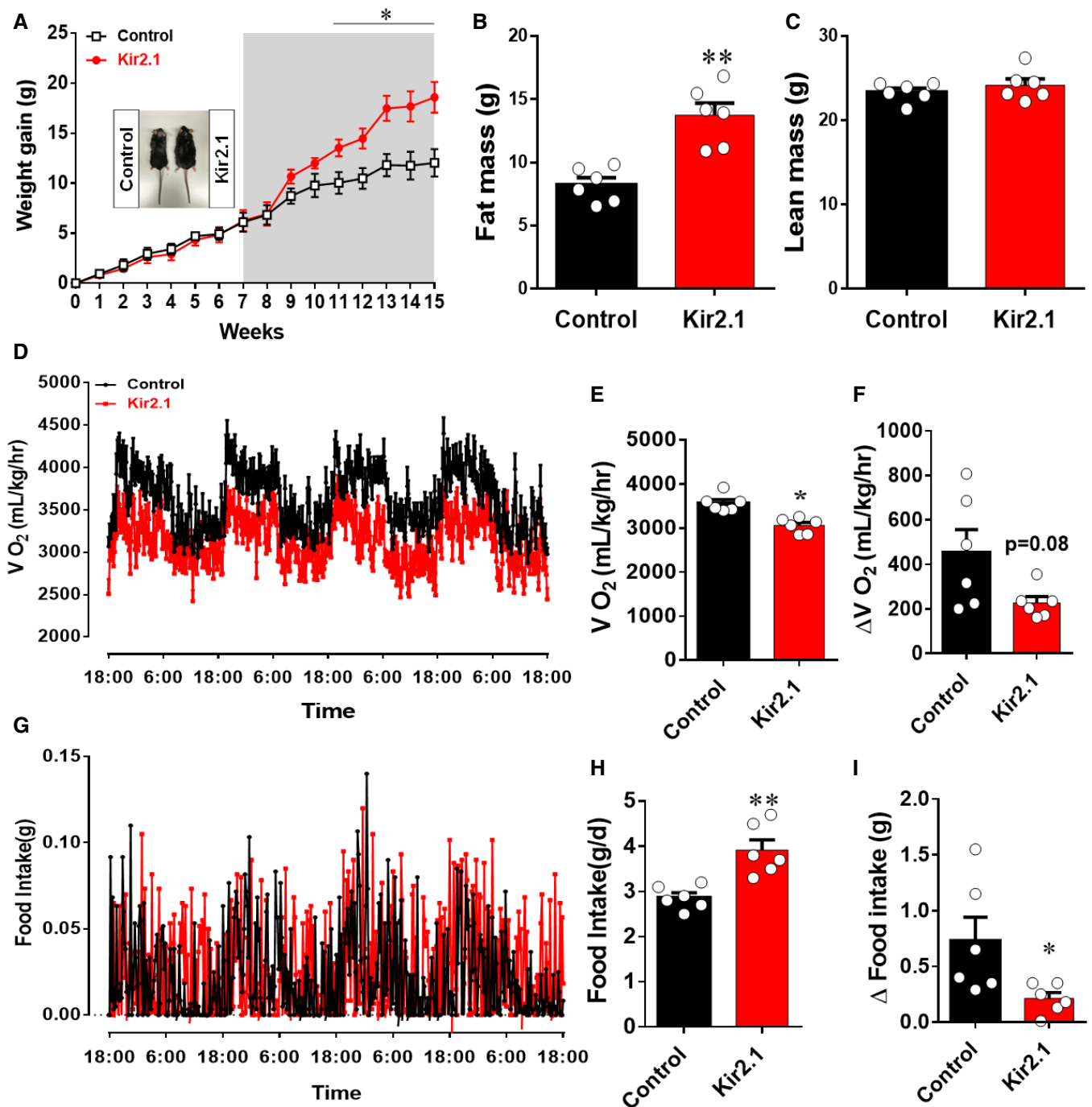


Figure 5. Clamping PVH CRH neuron activity at low levels causes diet-induced obesity.

A–I CRH-Cre male mice received stereotaxic delivery of AAV-EF1a-DIO-Kir2.1-P2A-dTomato or control AAV-Flex-mCherry vectors at 7–8 weeks of age and were maintained on chow diet for 7 weeks before switching to HFD. Weekly body weight gain after viral delivery (A, $*P < 0.0001$, unpaired Student's *t*-test), and measurements of fat mass (B, $**P = 0.0006$, unpaired Student's *t*-test) and lean mass (C, $P = 0.3728$, unpaired Student's *t*-test) at 15 weeks after viral delivery. (D–F) Measurements of energy expenditure during the 7th week after viral delivery. Comparison of real-time O_2 consumption traces during the 4-day measurement period (D), of average O_2 consumption between the two groups (E, $*P = 0.0007$, unpaired Student's *t*-test), and of the difference between day and night periods between the two groups (F, $P = 0.0791$, unpaired Student's *t*-test). (G–I) Measurements of feeding during the 7th week after viral delivery. Comparison of real-time feeding traces during the 4-day measurement period (G), of average food intake between the two groups (H, $**P = 0.0019$, unpaired Student's *t*-test), and of the difference in food intake between day and night periods between the two groups (I, $*P = 0.0363$, unpaired Student's *t*-test). $n = 6$ each. All data presented as mean \pm SEM.

Source data are available online for this figure.

neurons may serve as a primary neural substrate in mediating converging effects on obesity development by HFD feeding and chronic stress.

Materials and Methods

Animal care

Mice were housed at 21–22°C with a 12-h light/12-h dark cycle with standard pellet chow and water provided *ad libitum* unless otherwise noted for fasting experiments. Animal care and procedures were approved by the University of Texas Health Science Center at Houston Institutional Animal Care and Use Committee. CRH-Cre mice were purchased from the Jax lab and described and confirmed to express Cre in PVH CRH neurons previously [10,46]. Additionally, in most breeding pairs, either male or female breeders (or both) contained the Ai9 reporter gene (*Rosa-LSL-tdTomato*) to allow RFP expression in the presence of cre recombination 2. The HFD used in this study were purchased from Research Diet (D12492). All study subjects were littermates and randomly distributed between study groups. Group size was estimated based on relevant literature reports and differences in average between groups from pilot studies. All mice that were used for stereotaxic injections were at least 8–10 weeks old.

Surgeries and viral constructs

Stereotaxic surgeries to deliver viral constructs and for optical fiber implantation were performed as previously described. Briefly, mice were anesthetized with a ketamine/xylazine cocktail (100 mg/kg and 10 mg/kg, respectively), and their heads were affixed to a stereotaxic apparatus. Viral vectors were delivered through a 0.5 μ l syringe (Neuros Model 7000.5 KH, point style 3; Hamilton, Reno, NV, USA) mounted on a motorized stereotaxic injector (Quintessential Stereotaxic Injector; Stoelting, Wood Dale, IL, USA) at a rate of 30 nl/min. Viral preparations were titered at more than $\sim 1,012$ particles/ml. Viral delivery was targeted to the PVH (150 nl/side; anteroposterior [AP]: -0.9 mm; mediolateral [ML]: ± 0.1 mm; dorsoventral [DV]: -4.8 mm). AAV-Flex-GCaMP6m, AAV-EF1a-Flex-EGFP-P2A-mNachBac, or AAV-EF1a-DIO-Kir2.1-P2A-dTomato were delivered bilaterally into PVH of CRH-Cre mice. Two mutations (E224G and Y242F) were made in the Kir2.1 construct so that its activity will be less rectified by membrane potentials [32], thereby more effective in reducing neuron activity. AAV-Flex-GFP and AAV-Flex-mCherry injections were used as a control group. All viral vectors were either serotype 5 or DJ8, and provided through the Neuroconnectivity Core of Baylor College of Medicine with titer more than 1×10^{12} GC/ml. Behavioral testing was conducted following a minimum 4-week recovery period post-surgery.

Brain slice electrophysiological recordings

Mice were given an overdose of Avertin and then perfused intracardially with ice-cold cutting solution containing (in mM) 212 sucrose, 3 KCl, 1.25 NaH_2PO_4 , 26 NaHCO_3 , 7 MgCl_2 , and 10 glucose. Whole brain was excised quickly and immediately

immersed into ice-cold cutting solution. Coronal brain slices (250–300 μ m) containing the PVH from mice that had received stereotaxic injections of AAV-EF1a-Flex-EGFP-P2A-mNachBac, AAV-EF1a-DIO-Kir2.1-P2A-dTomato, or AAV-Flex-GFP to PVH at least 4 weeks prior to the recording were cut in oxygenized, ice-cold cutting solution. Slices were incubated for 60 min in artificial cerebrospinal fluid (aCSF) containing (in mM) 125 NaCl, 2.5 KCl, 1 MgCl_2 , 2 CaCl_2 , 1.25 NaH_2PO_4 , 25 NaHCO_3 , and 11 D -glucose bubbling with 95% O_2 /5% CO_2 , at 32–34°C, for recovery. Individual slices were transferred to a recording chamber mounted on an upright microscope (Olympus BX51WI) and continuously superfused (2 ml/min) with aCSF warmed to 32–34°C by passing it through a feedback-controlled in-line heater (TC-324B; Warner Instruments). Cells were visualized through a 40 \times water-immersion objective with differential interference contrast (DIC) optics and infrared illumination. Fluorescent-guided whole-cell patch clamp recordings were performed with a MultiClamp 700B amplifier (Axon Instruments). Patch pipettes were 3–5 $\text{M}\Omega$ when filled with an internal solution containing (in mM) 145 K Glu , 10 HEPES, 0.2 EGTA, 1 MgCl_2 , 4 Mg-ATP , 0.3 $\text{Na}_2\text{-GTP}$, and 10 $\text{Na}_2\text{-Phosphocreatine}$ (pH 7.3 adjusted with KOH; 295 mOsm). The whole-cell patch clamp recording was initiated by rupturing the plasma membrane of the cell voltage-clamped at -60 mV. Immediately after the formation of the whole-cell configuration, the clamp mode was switched to current clamp and the current injection was set to zero, membrane potential and spontaneous firing were recorded before a negative current pulse was applied to measure the input resistance, and a series of current steps were used to detect the action potential rheobase (the minimal injected current required for the generation of an action potential). Voltage clamp recordings were performed following current clamp recordings. The junction potential was not corrected throughout the study.

Body weight, food intake, and energy expenditure

Body weight studies

Weekly body weight was monitored on all genotypes mice fed standard mouse chow (Teklad F6 Rodent Diet 8664, 4.05 kcal/g, 3.3 kcal/g metabolizable energy, 12.5% kcal from fat, Harlan Teklad, Madison, WI) from 4 to 20 weeks of age. Body composition (fat mass and lean mass) was measured at indicated times by using the Echo-MRI system (EchoMRI, Houston, TX). Littermate subjects were randomly assigned to study groups with a comparable initial body weight between groups. Animal IDs were blinded when body weight data were collected.

Food intake measurements

In young age mice, all study subjects were individually housed after weaning, and daily food intake was monitored for 1 week after 3 days acclimation. Body weights of these mice were also recorded at the beginning and end of the measurement period. In adult age mice (19–20 weeks old), all study subjects were pre-acclimated for at least 1 week by single housing, and then, daily food intake was monitored for 1 week. For both age groups, daily food intakes were calculated as the mean values of the 1-week measurement. All housing cages were changed daily during the measurement period.

Energy expenditure analysis

Energy expenditure was measured by oxygen consumption by indirect calorimetry. Individual housed mice maintained on chow diet at 4–5 weeks old were placed at room temperature (22–24°C) in chambers of a Comprehensive Lab Animal Monitoring System (CLAMS, Columbus Instruments, Columbus, OH). Food and water were provided *ad libitum*. Mice were acclimatized in the chambers for at least 48 h prior to data collection.

Fast-refeeding studies

Mice received injections of viral vectors were used for fasting and fast-refeeding studies at least 4 weeks after viral delivery. For the HFD condition, mice were switched to HFD and maintained on HFD for at least another 4 weeks of period before fasting-refeeding studies. For the fast group, mice were fasted for 24 h and for the fast-refeeding group, mice were allowed to eat food *ad libitum* for 2 h after 24-h fasting. All mice were handled daily for a week to reduce stress levels before transcardial perfusion.

Behavioral assays

All behavioral assays were performed before body weight became different between groups fed on chow, and the animal ID was blinded when behavior tests were conducted.

Open field test

The apparatus consists of a white Plexiglas box and is brightly illuminated (120 lx). Each mouse was placed in the corner of the apparatus to initiate a 20-min test session. A camera (Noldus, Leesburg, VA, USA) mounted above the apparatus monitors the mice, and the track of its movements was recorded, which were analyzed by EthoVision XT software. Time spent in the center was recorded and subsequently analyzed, longer times spent exploring the arena in the center seen as less anxiety-like behaviors.

Elevated-plus maze

Elevated-plus maze that consists of two open and two closed arms was positioned 50 cm above the floor (Kinder Scientific, Poway, CA, USA). Mice were placed on the central facing an open arm, to initiate a 10-min session test. The time spent in the open or closed arms was recorded and analyzed by Kinder Scientific Motor Monitor software.

Light/dark room test

The light/dark room test apparatus consists of two same space parts, light room and the dark room (Kinder Scientific, Poway, CA, USA). Mice were placed in the center of apparatus with an opening to the both side, to initiate a 10-min session test. The time spent in the light room was recorded and analyzed by Kinder Scientific Motor Monitor software.

Brain tissue preparation, immunohistochemistry, imaging, and post hoc analysis

After behavioral experiments were completed, study subjects were anesthetized with a ketamine/xylazine cocktail (100 and 10 mg/kg, respectively) and subjected to transcardial perfusion. During

perfusion, animals were flushed with 20 ml of saline prior to fixation with 20 ml of 10% buffered formalin. Freshly fixed brains were then extracted and placed in 10% buffered formalin in 4°C overnight for post-fixation. The next day, brains were transferred to 30% sucrose solution and allowed to rock at room temperature for 24 h prior to sectioning. Brains were frozen and sectioned into 30 µm slices with a sliding microtome and mounted onto slides for *post hoc* visualization of injection sites and cannula placements. Primary antibodies used were rabbit mAb against c-Fos from cell signaling technology (#2250, 1:1,000 dilution) and rabbit polyclonal antibody against CRH from Peninsula Laboratories International Inc. (Cat. No: T-4037, 1:1,000 dilution). Mice with missed injections to the PVH were excluded from data analysis. Representative pictures of PVH injection sites were visualized with confocal microscopy (Leica TCS SP5; Leica Microsystems, Wetzlar, Germany).

In vivo fiber photometry experiments

Corticotropin-releasing hormone-Cre mice with specific delivery of AAV-Flex-GCaMP6m [30] to the PVH and optic fiber implantation targeting PVH neurons were used for the *in vivo* fiber photometry Ca²⁺ imaging studies. The GCaMP6m virus was provided by the Baylor Neuroconnectivity Core. The experiments were conducted at least 4 weeks after the surgery. All fiber photometry was conducted using a Doric Lenses setup, with an LED Driver controlling two connectorized LEDs (405 and 465 nm) routed through a five port Fluorescence MiniCube (Order code: FMC5_AE(405)_AF(420-450)_E1(460-490)_F1(500-550)_S) to deliver excitation light for calcium-independent and calcium-dependent signals to the implanted optic fiber simultaneously. Emitted light was received through the MiniCube and split into two bands—420–450 nm (autofluorescence—calcium-independent signal) and 500–550 nm (GCaMP6 signal—calcium-dependent signal). Each band was collected by a Newport 2151 Visible Femtowatt Photoreceiver module (photometer) with an add-on fiber-optic adaptor. Output analog signal was converted to digital signal through the fiber photometry console and recorded using the “Analog-In” function on Doric Studios (V4.1.5.2). Mice were acclimated to the behavioral chamber for at least 15 min prior to the beginning of each testing session. After baseline recording for 10 s, water spray was started by spraying one time with water toward the head of mice with a sprayer and the recording will continue for about 2 min. The signal from the independent channel was used to control for potential fiber slippage or other mechanical issues.

Data were acquired through Doric Studios V4.1.5.2. and saved as comma-separated files (header was deleted) at a sampling rate of 1 kS/s. For water spray, the baseline was calculated from 10 s prior to stimulus onset, to 20 s after stimulus onset. For Dex injections, 1.5 min prior to IP injection was used to calculate baseline, and this period was averaged and compared to a 1.5-min time segment occurring 5 min after IP injection.

Statistics

GraphPad Prism 7.00 (GraphPad Software, Inc., La Jolla, CA, USA) was used for all statistical analyses and construction of graphs except as described above. Single variable comparisons were made by paired or unpaired two-tailed Student's *t*-tests, or one-way

ANOVA followed by Tukey's multiple comparison *post hoc* tests. Error bars in graphs were represented as \pm SEM.

Expanded View for this article is available online.

Acknowledgements

This study was supported by NIH R01 DK114279 and R21 NS 108091 to QT; NIH R01DK117281 and R01DK101379 to YoX; R01DK109934 and DOD W81XWH-19-1-0429 to B.R.A. and Q.T.; and NIH R01MH117089 and McKnight Foundation to M.X. We also acknowledge the Neuroconnectivity Core funded by NIH IDRC grant 1 U54 HD083092 and Baylor College of Medicine Gene Vector Core for providing AAV vectors. C.Z was supported by the Graduate Student Overseas Study Program (2017LHPY024) from South China Agricultural University. We would like to acknowledge the Tong lab members for helpful discussion and Dr. Zhengmei Mao for help with microscopy. QT is the holder of Cullen Chair in Molecular Medicine at McGovern Medical School.

Author contributions

CZ conducted the research with help from JBT and ZJ, YuX, and RMC; MX, BRA, GS, Z-LC, and YoX provided essential reagents; QT, QJ, and CZ conceived and designed the studies, and wrote the manuscript with significant inputs from GS, YoX, and BRA.

Conflict of interest

The authors declare that they have no conflict of interest.

References

- Sominsky L, Spencer SJ (2014) Eating behavior and stress: a pathway to obesity. *Front Psychol* 5: 434
- Tomiya AJ (2019) Stress and obesity. *Annu Rev Psychol* 70: 703–718
- Razzoli M, Pearson C, Crow S, Bartolomucci A (2017) Stress, overeating, and obesity: insights from human studies and preclinical models. *Neurosci Biobehav Rev* 76: 154–162
- Flier JS (2004) Obesity wars: molecular progress confronts an expanding epidemic. *Cell* 116: 337–350
- Hatori M, Vollmers C, Zarrinpar A, DiTacchio L, Bushong EA, Gill S, Leblanc M, Chaix A, Joens M, Fitzpatrick JA et al (2012) Time-restricted feeding without reducing caloric intake prevents metabolic diseases in mice fed a high-fat diet. *Cell Metab* 15: 848–860
- Pecoraro N, Reyes F, Gomez F, Bhargava A, Dallman MF (2004) Chronic stress promotes palatable feeding, which reduces signs of stress: feedforward and feedback effects of chronic stress. *Endocrinology* 145: 3754–3762
- Bartolomucci A, Cabassi A, Govoni P, Ceresini G, Cero C, Berra D, Daddomo H, Franceschini P, Dell'Omo G, Parmigiani S et al (2009) Metabolic consequences and vulnerability to diet-induced obesity in male mice under chronic social stress. *PLoS ONE* 4: e4331
- Kuo LE, Czarnecka M, Kitlinska JB, Tilan JU, Kvetnansky R, Zukowska Z (2008) Chronic stress, combined with a high-fat/high-sugar diet, shifts sympathetic signaling toward neuropeptide Y and leads to obesity and the metabolic syndrome. *Ann N Y Acad Sci* 1148: 232–237
- Tsai SF, Wu HT, Chen PC, Chen YW, Yu M, Tzeng SF, Wu PH, Chen PS, Kuo YM (2018) Stress aggravates high-fat-diet-induced insulin resistance via a mechanism that involves the amygdala and is associated with changes in neuroplasticity. *Neuroendocrinology* 107: 147–157
- Wamsteeker Cusulin JI, Fuzesi T, Watts AG, Bains JS (2013) Characterization of corticotropin-releasing hormone neurons in the paraventricular nucleus of the hypothalamus of Crh-IRES-Cre mutant mice. *PLoS ONE* 8: e64943
- Gold PW (2015) The organization of the stress system and its dysregulation in depressive illness. *Mol Psychiatry* 20: 32–47
- Ulrich-Lai YM, Ryan KK (2014) Neuroendocrine circuits governing energy balance and stress regulation: functional overlap and therapeutic implications. *Cell Metab* 19: 910–925
- Ulrich-Lai YM, Herman JP (2009) Neural regulation of endocrine and autonomic stress responses. *Nat Rev Neurosci* 10: 397–409
- Fuzesi T, Daviu N, Wamsteeker Cusulin JI, Bonin RP, Bains JS (2016) Hypothalamic CRH neurons orchestrate complex behaviours after stress. *Nat Commun* 7: 11937
- Zhang R, Asai M, Mahoney CE, Joachim M, Shen Y, Gunner G, Majzoub JA (2017) Loss of hypothalamic corticotropin-releasing hormone markedly reduces anxiety behaviors in mice. *Mol Psychiatry* 22: 733–744
- Okamoto S, Sato T, Tateyama M, Kageyama H, Maejima Y, Nakata M, Hirako S, Matsuo T, Kyaw S, Shiuchi T et al (2018) Activation of AMPK-regulated CRH neurons in the PVH is sufficient and necessary to induce dietary preference for carbohydrate over fat. *Cell Rep* 22: 706–721
- Huang Q, Rivest R, Richard D (1998) Effects of leptin on corticotropin-releasing factor (CRF) synthesis and CRF neuron activation in the paraventricular hypothalamic nucleus of obese (ob/ob) mice. *Endocrinology* 139: 1524–1532
- Pivonello R, De Leo M, Cozzolino A, Colao A (2015) The treatment of Cushing's disease. *Endocr Rev* 36: 385–486
- Shah BP, Vong L, Olson DP, Koda S, Krashes MJ, Ye C, Yang Z, Fuller PM, Elmquist JK, Lowell BB (2014) MC4R-expressing glutamatergic neurons in the paraventricular hypothalamus regulate feeding and are synaptically connected to the parabrachial nucleus. *Proc Natl Acad Sci USA* 111: 13193–13198
- Li C, Navarrete J, Liang-Guallpa J, Lu C, Funderburk SC, Chang RB, Liberles SD, Olson DP, Krashes MJ (2019) Defined paraventricular hypothalamic populations exhibit differential responses to food contingent on caloric state. *Cell Metab* 29: 681–694.e5
- Kentish SJ, Vincent AD, Kennaway DJ, Wittert GA, Page AJ (2016) High-fat diet-induced obesity ablates gastric vagal afferent circadian rhythms. *J Neurosci* 36: 3199–3207
- Honma K, Hikosaka M, Mochizuki K, Goda T (2016) Loss of circadian rhythm of circulating insulin concentration induced by high-fat diet intake is associated with disrupted rhythmic expression of circadian clock genes in the liver. *Metabolism* 65: 482–491
- Kalyani M, Hasselfeld K, Janik JM, Callahan P, Shi H (2016) Effects of high-fat diet on stress response in male and female wildtype and prolactin knockout mice. *PLoS ONE* 11: e0166416
- Auvinen HE, Romijn JA, Biermasz NR, Pijl H, Havekes LM, Smit JW, Rensen PC, Pereira AM (2012) The effects of high fat diet on the basal activity of the hypothalamus-pituitary-adrenal axis in mice. *J Endocrinol* 214: 191–197
- Naef L, Gratton A, Walker CD (2013) Exposure to high fat during early development impairs adaptations in dopamine and neuroendocrine responses to repeated stress. *Stress* 16: 540–548
- Ahima RS, Prabakaran D, Flier JS (1998) Postnatal leptin surge and regulation of circadian rhythm of leptin by feeding. Implications for energy homeostasis and neuroendocrine function. *J Clin Invest* 101: 1020–1027
- Singru PS, Wittmann G, Farkas E, Zseli G, Fekete C, Lechan RM (2012) Refeeding-activated glutamatergic neurons in the hypothalamic

- paraventricular nucleus (PVN) mediate effects of melanocortin signaling in the nucleus tractus solitarius (NTS). *Endocrinology* 153: 3804–3814
28. Kim J, Lee S, Fang YY, Shin A, Park S, Hashikawa K, Bhat S, Kim D, Sohn JW, Lin D et al (2019) Rapid, biphasic CRF neuronal responses encode positive and negative valence. *Nat Neurosci* 22: 576–585
 29. Chen TW, Wardill TJ, Sun Y, Pulver SR, Renninger SL, Baohan A, Schreiter ER, Kerr RA, Orger MB, Jayaraman V et al (2013) Ultrasensitive fluorescent proteins for imaging neuronal activity. *Nature* 499: 295–300
 30. Xu Y, Lu Y, Cassidy RM, Mangieri LR, Zhu C, Huang X, Jiang Z, Justice NJ, Xu Y, Arenkiel BR et al (2019) Identification of a neurocircuit underlying regulation of feeding by stress-related emotional responses. *Nat Commun* 10: 3446
 31. Tasker JG, Di S, Malcher-Lopes R (2006) Minireview: rapid glucocorticoid signaling via membrane-associated receptors. *Endocrinology* 147: 5549–5556
 32. Xue M, Atallah BV, Scanziani M (2014) Equalizing excitation-inhibition ratios across visual cortical neurons. *Nature* 511: 596–600
 33. Patel JM, Swanson J, Ung K, Herman A, Hanson E, Ortiz-Guzman J, Selever J, Tong Q, Arenkiel BR (2019) Sensory perception drives food avoidance through excitatory basal forebrain circuits. *Elife* 8: e44548
 34. Watts AG, Tanimura S, Sanchez-Watts G (2004) Corticotropin-releasing hormone and arginine vasopressin gene transcription in the hypothalamic paraventricular nucleus of unstressed rats: daily rhythms and their interactions with corticosterone. *Endocrinology* 145: 529–540
 35. Laryea G, Schutz G, Muglia LJ (2013) Disrupting hypothalamic glucocorticoid receptors causes HPA axis hyperactivity and excess adiposity. *Mol Endocrinol* 27: 1655–1665
 36. Wei W, Pham K, Gammons JW, Sutherland D, Liu Y, Smith A, Kaczorowski CC, O'Connell KM (2015) Diet composition, not calorie intake, rapidly alters intrinsic excitability of hypothalamic AgRP/NPY neurons in mice. *Sci Rep* 5: 16810
 37. Suyama S, Ralevski A, Liu ZW, Dietrich MO, Yada T, Simonds SE, Cowley MA, Gao XB, Diano S, Horvath TL (2017) Plasticity of calcium-permeable AMPA glutamate receptors in Pro-opiomelanocortin neurons. *Elife* 6: e25755
 38. Mazier W, Saucisse N, Simon V, Cannich A, Marsicano G, Massa F, Cota D (2019) mTORC1 and CB1 receptor signaling regulate excitatory glutamatergic inputs onto the hypothalamic paraventricular nucleus in response to energy availability. *Mol Metab* 28: 151–159
 39. Sutton AK, Myers MG Jr, Olson DP (2016) The role of PVH circuits in leptin action and energy balance. *Annu Rev Physiol* 78: 207–221
 40. Hryhorczuk C, Decarie-Spain L, Sharma S, Daneault C, Rosiers CD, Alquier T, Fulton S (2017) Saturated high-fat feeding independent of obesity alters hypothalamus-pituitary-adrenal axis function but not anxiety-like behaviour. *Psychoneuroendocrinology* 83: 142–149
 41. Brown ER, Sawchenko PE (1997) Hypophysiotropic CRF neurons display a sustained immediate-early gene response to chronic stress but not to adrenalectomy. *J Neuroendocrinol* 9: 307–316
 42. Finger BC, Dinan TG, Cryan JF (2012) The temporal impact of chronic intermittent psychosocial stress on high-fat diet-induced alterations in body weight. *Psychoneuroendocrinology* 37: 729–741
 43. Sanghez V, Razzoli M, Carobbio S, Campbell M, McCallum J, Cero C, Ceresini G, Cabassi A, Govoni P, Franceschini P et al (2013) Psychosocial stress induces hyperphagia and exacerbates diet-induced insulin resistance and the manifestations of the Metabolic Syndrome. *Psychoneuroendocrinology* 38: 2933–2942
 44. Vliementhart J, Noppe G, van Rossum EF, Koper JW, Raat H, van den Akker EL (2016) Socioeconomic status in children is associated with hair cortisol levels as a biological measure of chronic stress. *Psychoneuroendocrinology* 65: 9–14
 45. Watts AG, Swanson LW (1989) Diurnal variations in the content of precorticotropin-releasing hormone messenger ribonucleic acids in the hypothalamic paraventricular nucleus of rats of both sexes as measured by *in situ* hybridization. *Endocrinology* 125: 1734–1738
 46. Taniguchi H, He M, Wu P, Kim S, Paik R, Sugino K, Kvitsiani D, Fu Y, Lu J, Lin Y et al (2011) A resource of Cre driver lines for genetic targeting of GABAergic neurons in cerebral cortex. *Neuron* 71: 995–1013